A Database of *Caenorhabditis elegans* Locomotion and Body Posture Phenotypes for the Peripheral Neuropathy Model

Ki Wha Chung[1], Ju Seong Kim[1], and Kyung Suk Lee[2,*]

[1]Department of Biological Sciences, Kongju National University, Gongju 32588, Korea, [2]Department of Physics Education, Kongju National University, Gongju 32588, Korea
*Correspondence: leeks@kongju.ac.kr
https://doi.org/10.14348/molcells.2020.0178
www.molcells.org

Inherited peripheral neuropathy is a heterogeneous group of peripheral neurodegenerative disorders including Charcot–Marie–Tooth disease. Many peripheral neuropathies often accompany impaired axonal construction and function. To study the molecular and cellular basis of axon-defective peripheral neuropathy, we explore the possibility of using *Caenorhabditis elegans*, a powerful nematode model equipped with a variety of genetics and imaging tools. In search of potential candidates of *C. elegans* peripheral neuropathy models, we monitored the movement and the body posture patterns of 26 *C. elegans* strains with disruption of genes associated with various peripheral neuropathies and compiled a database of their phenotypes. Our assay showed that movement features of the worms with mutations in *HSPB1*, *MFN2*, *DYNC1H1*, and *KIF1B* human homologues are significantly different from the control strain, suggesting they are viable candidates for *C. elegans* peripheral neuropathy models.

Keywords: *Caenorhabditis elegans*, disease model, locomotion, peripheral neuropathy

INTRODUCTION

Inherited peripheral neuropathies (IPNs) are a broad ranged group of genetically and clinically heterogeneous neurodegenerative disorders affecting the peripheral nervous system (PNS) with variable clinical patterns and a number of different genetic causes. Depending on the types of damaged peripheral nerves, IPNs are divided into Charcot–Marie–Tooth disease (CMT), distal hereditary motor neuropathy (dHMN), hereditary sensory autonomous neuropathy, hereditary neuropathy with pressure palsies (HNPP), and several other disorders with symptoms of muscle weakness, numbness, and pain (England and Asbury, 2004). CMT, also called hereditary motor and sensory neuropathy, is the most common peripheral neuropathy with gait disturbance, muscle weakness, and sensory defects at the extremities (Schwartz, 2019). There are demyelinating peripheral neuropathies such as CMT type 1 and axonal peripheral neuropathies such as CMT type 2. Moreover, they are further classified into many subtypes based on genetic and phenotypic classification (Pareyson et al., 2017).

While characterization of clinical features, linkage analysis, and whole exome sequencing of the study participants have uncovered a number of novel causative genes (Nam et al., 2016), researchers also developed animal models to confirm genetic causes of clinical phenotypes. First introduced 20 years ago, mouse models have been extensively used to study various causative genes such as *PMP22* (CMT1A, CMT1E, and HNPP), *MPZ* (CMT1B), *HSPB1* (CMT2F, dHMN2B),

MTMR2 (CMT4B), and so on (Hong et al., 2016; Tanaka and Hirokawa, 2002). In recent years, zebrafish models were introduced to IPN studies (Bragato et al., 2016; Hong et al., 2016; Won et al., 2019). These animal models are not only useful for dissecting the role of causative genes but also for investigation of therapeutic targets. For example, transgenic mice with a mutation in the *HSPB1* gene, which causes CMT2F and dHMN2B (Evgrafov et al., 2004), were assayed for the therapeutic effect of HDAC6 inhibitors, and the treatment effectively reversed axonal loss in these mice (d'Ydewalle et al., 2011).

Axons in *Drosophila melanogaster* or *Caenorhabditis elegans* are not surrounded by myelin sheaths or Schwann cells, and therefore they are not suitable models for demyelinating peripheral neuropathies, but they still can be used as a model system for peripheral neuropathies characterized by axonal impairment. The causative genes of axonal neuropathies examined using the *Drosophila* model so far include *GARS1*, *GDAP1*, *MFN2*, and *YARS1* (Yamaguchi and Takashima, 2018).

C. elegans models have not been employed as much as the other animal models. Recently, however, there was a report that disruption of *fzo-1*, a *C. elegans* homologue for *MFN2*, induced differences in mitochondrial morphology and deficits in worm movement (Byrne et al., 2019). *MFN2*, a key player in mitochondrial activities (Long et al., 2019), is a causative gene for the axonal CMT2A and HMSN6A characterized by defects in mitochondrial dynamics and axonal transport, and this result therefore suggests the utility of *C. elegans* models for axonal peripheral neuropathies.

In an effort to find potential *C. elegans* peripheral neuropathy models, we made a list of *C. elegans* homologues of currently known causative IPN genes. We then examined the motor behaviors of the worm strains with mutations in these genes and searched for those that show the deficits, as the worm's locomotion and body posture might be substantially matched by the IPN phenotypes. This makes monitoring their movement a relatively simple yet useful experimental approach for neurogenetics in worms (Yemini et al., 2013).

To do so, we made a simplified version of WormTracker (Yemini et al., 2013) and monitored the motor behaviors of 26 different worm strains, and compiled a database of their behavioral features. Our assay then shows that the worms with mutations in *HSPB1*, *MFN2*, *DYNC1H1*, and *KIF1B* homologues evidently exhibit phenotypes of abnormal movement, suggesting them as candidates for *C. elegans* peripheral neuropathy models.

MATERIALS AND METHODS

Preparation of worms
C. elegans strains were cultured using standard techniques (Brenner, 1974). Worms were synchronized and grown until they reached adulthood at 25°C. The experiments were performed when they reached adulthood and started laying eggs. For the measurement, 10 to 12 individuals were moved to a new nematode growth medium (NGM) plate 10 min before recording. To control the effect of the medium on worms' movement, we made fresh plates one day before the

experiment. In case the homozygotes are lethal (*rab-7, tfg-1, hars-1,* and *yars-1*), we used only the progenies of heterozygotes for the experiment, after confirming they are heterozygous by checking their segregants.

Image analysis and statistical analysis
We recorded 1,200 images for 10 individuals for each experiment. To analyze these images automatically, we wrote custom MATLAB (MATLAB2013b; Mathworks, USA) scripts that extract the movement trajectories (Fig. 1A) and the body-skeleton curves (Fig. 1B) of individuals. From the trajectory and the body-skeleton curve, we quantified 104 behavioral and moving features.

The distribution of each feature of a mutant was compared to that of the control strain (N2) in order to determine a distribution-free overlapping index η (Pastore and Calcagnì, 2019). Taking into consideration that the overlap between two different normal distributions follows a normal distribution (Inman and Bradley, 1989), we converted the overlapping index η to the *P* value of a null hypothesis that the two distributions are not different. Following the same procedures in the WormTracker (Yemini et al., 2013), we checked for the significance at $P \le 0.01$ and calculated the *q*-value, the positive false discovery rate (Storey, 2002).

A statistical analysis was also performed using a custom written MATLAB script. All MATLAB scripts will be available upon request.

RESULTS

C. elegans strains with mutation of homologues of the IPN genes
To find *C. elegans* strains (with disruption of a gene) associat-
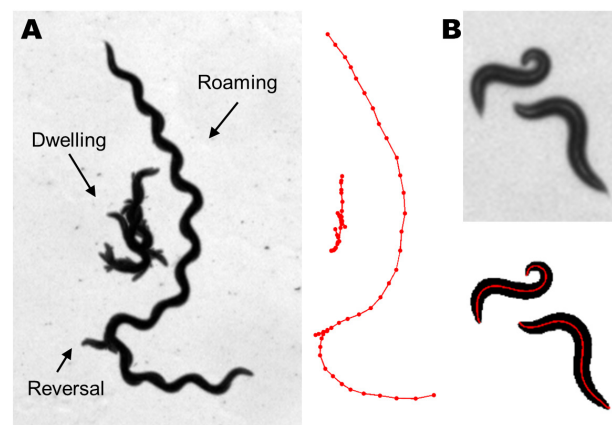
Fig. 1. Measurement and quantification of worm's behavior. (A) The images recorded using our setup. Forty frames were combined to show the movement of worms for 20 s. The worm in the center is dwelling, while the other is roaming. The latter shows reversal. Red curves are the trajectories obtained through automated image analysis. (B) A zoomed-in view of a raw image of two worms. Through image analysis, the raw image (top) is converted to a black-and-white image (bottom). Red curves indicate the body-skeleton curves we calculated.

Table 1. A list of causative genes of axonal peripheral neuropathies and *C. elegans* homologues

Gene	Protein	IPN phenotype (MIM#[a])	Inheritance	*C. elegans* homologues
AARS1	Alanyl-tRNA synthetase	CMT2N (613287)	AD	aars-2, aars-1
DGAT2	Diacylglycerol O-acyltransferase 2	CMT2 (-)	AD	dgat-2, dgtr-1, K07B1.4, Y53G8B.2
DHTKD1	Dehydrogenase E1 and transkotolase domains-containing protein 1	CMT2Q (615025)	AD	ogdh-2, ogdh-1
DNM2	Dynamin 2	CMT2M, CMTDIB (606482)	AD	dyn-1, drp-1
DYNC1H1	Dynein, cytoplasmic 1, heavy chain 1	CMT2O (614228)	AD	dhc-1, che-3
GARS1	Glycyl-tRNA synthetase	CMT2D (601472)	AD	gars-1
		dHMN5A (600794)	AD	
GDAP1	Ganglioside-induced differentiation-associated protein 1	CMT2K (607831)	AD	exc-4, exl-1, gst-43, Y53G8B.1
		CMTRIA (608340)	AR	
		CMT4A (214400)	AR	
HARS1	Histidyl-tRNA synthetase	CMT2W (616625)	AD	hars-1
HSPB1	Heat shock protein 27	CMT2F (606595)	AD	hsp-12.1, hsp-12.2, hsp-12.3, hsp-12.6, hsp-16.1,
		dHMN2B (608634)	AD	hsp-16.2, hsp-16.11, hsp-16.41, hsp-16.48,
HSPB3	HSP27-like protein	dHMN2C (613376)	AD	hsp-16.49, hsp-17, hsp-25, hsp-43, sip-1, F08H9.3,
HSPB8	Heat shock protein 22	CMT2L (608673)	AD	F08H9.4, Y55F3BR.6, ZK1128.7
		dHNM2A (158590)	AD	
KIF1B	Kinesin family member 1B	CMT2A1 (118210)	AD	unc-104
LMNA	Lamin A/C	CMT2B1 (605588)	AR	lmn-1, ifa-1, ifa-3, ifa-4, ifb-2, ifc-1, ifc-2, ifp-1, mua-6
LRSAM1	Leucine rich repeat and sterile alpha motif 1	CMT2P (614436)	AD, AR	N/A
MARS1	Methionyl-tRNA synthetase	CMT2U (616280)	AD	mars-1
MED25	Mediator complex subunit 25	CMT2B2 (605589)	AR	N/A
MFN2	Mitofusin 2	CMT2A2A (609260)	AD	fzo-1
		CMT2A2B (617087)	AR	
		HMSN6A (601152)	AD	
MME	Membrane metallo-endopeptidase	CMT2T (617017)	AD, AR	nep-1, nep-2, nep-3, nep-4, nep-5, nep-6, nep-7, nep-8, nep-9, nep-10, and 16 other genes
MORC2	MORC family CW-type zinc finger 2	CMT2Z (616688)	AD	morc-1
MPZ	Myelin protein zero	CMT1B (118200)	AD	N/A
		CMT2I (607677)	AD	
		CMT2J (607736)	AD	
		HMSN3 (145900)	AD	
NEFL	Neurofilament, light polypeptide	CMT1F (607734)	AD, AR	ifa-1, ifa-3, ifa-4, ifb-1, ifb-2, mua-6
		CMT2E (607684)	AD	
		CMTDIG (617882)	AD	
PNKP	Polynucleotide kinase 3'-phosphatase	CMT2B2 (605589)	AR	F21D5.5
RAB7A	RAS-associated protein RAB7	CMT2B (600882)	AD	rab-7, rab-33, rab-37
TRIM2	Tripartite motif-containing protein 2	CMT2R (615490)	AR	nhl-1, nhl-2, nhl-3, ncl-1, lin-41
TRPV4	Transient receptor potential vanilloid 4	HMSN2C (606071)	AD	ocr-4, ocr-1, ocr-3, osm-9, ocr-2
VCP	Valosin containing protein	CMT2Y (616687)	AD	cdc-48.1, cdc-48.2, cdc-48.3, mac-1
TFG	TRK-fused gene	HMSNP (604484)	AD	tfg-1, Y71A12B.10
YARS1	Tyrosyl-tRNA synthetase	CMTDIC (608323)	AD	yars-1
FGD4	FYVE, RhoGEF and PH domain containing 4	CMT4H (609311)	AR	exc-5, frm-3
PMP2	Peripheral myelin protein 2	CMTDIG (618279)	AD	lbp-3, lbp-4, lbp-5, lbp-6, lbp-7, lbp-8, lbp-9
MTMR2	Myotubularin-related protein 2	CMT4B1 (601382)	AR	
SBF1	SET-binding factor 1	CMT4B3 (615284)	AR	mtm-1, mtm-3, mtm-5, mtm-6, mtm-9,
SBF2	SET-binding factor 2	CMT4B2 (604563)	AR	Y48G1C.10

IPN, inherited peripheral neuropathy; AD, autosomal dominant; AR, autosomal recessive.
[a]MIM numbers are obtained from the Online Mendelian Inheritance in Man (http://omim.org/).

ed with IPNs, we first identified the homologues of causative genes, and then looked up the databases of worm strains bearing the mutation of their homologues. In Table 1, we list human genes identified as underlying causes of the axonal peripheral neuropathies from the Inherited Neuropathy Variant Browser (http://hihg.med.miami.edu/code/http/cmt/public_html/) and recent studies (Lee et al., 2020; Pareyson et al., 2017; Yamaguchi and Takashima, 2018). We also listed their homologues in *C. elegans*, referring to the HUGO Gene Nomenclature Committee (HGNC; https://www.genenames.org/) Comparison of Orthology Predictions (HCOP) (Wright et al., 2005) and WormBase (https://wormbase.org/), a model organism information resource (Harris et al., 2020).

Next, we searched two worm strain databases, *Caenorhabditis* Genetics Center (CGC, University of Minnesota, USA) and National BioResource Project (NBRP) *C. elegans* (Tokyo Women's Medical University, Japan), for mutants of the *C. elegans* homologues of causative genes. Although not all genes had their mutant strains available, we could select 26 strains to monitor their motor behaviors (Table 2, Supplementary Fig. S1).

First, we included the mutants of *HSPB1* homologues, because *HSPB1* is one of the most studied causative genes for axonal peripheral neuropathies such as CMT2 and dHMN2B (Evgrafov et al., 2004; Schwartz, 2019), and relevant ani-

mal models would be valuable for developing therapeutic strategies such as HDAC6 inhibitors (d'Ydewalle et al., 2011; Kim et al., 2016; Schwartz, 2019). *GARS1*, which encodes glycyl-tRNA synthetase, was another gene of interest because several aminoacyl-tRNA synthetase genes had been linked to IPN (Antonellis et al., 2003; Jordanova et al., 2006; Lee et al., 2012; 2020; Vester et al., 2013). However, its mutant was not available, and therefore we included *hars-1*/*HARS1* and *yars-1*/*YARS1* in our assay instead. *fzo-1*/*MFN2* is also an interesting gene related to mitochondrial dynamics, because *MFN2* homologues have been one of the successful invertebrate model systems, as mentioned above (Byrne et al., 2019; Eschenbacher et al., 2012). For comparison, we also added several genes causing demyelinating peripheral neuropathies: *exc-5*/*FGD4*, *lbp-5*/*PMP2*, *mtm-1*, and *mtm-5*/*MTMR2*. Even though *exc-5* deficient mutant was associated with CMT4H, not the axonal type of CMT, it was one of the earliest *C. elegans* CMT models, due to the morphological similarity between the structural defects of its excretory canals and those in tubules in CMT4H patients (Mattingly and Buechner, 2011).

We preferred a homozygote with a mutation of a single gene of interest, but such strains were not always available. In the absence of such strains, a heterozygote or a strain with multiple mutations was examined to cover various subtypes

Table 2. A list of the worm strains used in this study

Human gene	*C. elegans* homologue	Strain	Genotype	Note
-	-	N2	*C. elegans* wild type	Wild type
HSPB1, HSPB3, HSPB8	hsp-12.1	RB2600	hsp-12.1(ok3622) I.	~400 bp deletion
	hsp-12.2	RB2612	hsp-12.2(ok3638) III.	~400 bp deletion
	hsp-12.3	VC2346	hsp-12.3(ok3095) IV.	533 bp deletion
	hsp-12.6	VC281	hsp-12.6(gk156) IV.	743 bp deletion
	hsp-16.2	VC475	hsp-16.2(gk249) V.	212 bp deletion
	hsp-16.41	tm1093	hsp-16.41(tm1093) V.	272 bp deletion (+ 13 bp insertion)
	hsp-16.48	RB791	hsp-16.48(ok577) V.	1803 bp deletion
	hsp-43	RB825	hsp-43(ok647) X.	1816 bp deletion
	sip-1	tm3624	sip-1(tm3624) I.	282 bp deletion
	F08H9.3	tm5012	F08H9.3(tm5012) V.	665 bp deletion (+ 25 bp insertion)
	F08H9.4	RB1604	F08H9.4&srz-97(ok1976) V.	1342 bp deletion
MFN2	fzo-1	CU5991	fzo-1(tm1133) II.	419 bp deletion (+ 14 bp insertion)
DYNC1H1	dhc-1	EU828	dhc-1(or195) I.	substitution (C > T; S3200L, S2268L for two isoforms)
KIF1B	unc-104	KG4386	unc-104(ce782) II.	substitution (G > A; G105E)
LMNA, NEFL	ifa-4	RB1483	ifa-4(ok1734) X.	711 bp deletion
	ifb-2	VC20740	ifb-2(gk963053) II.	deletion (million mutation project)
TRPV4	ocr-4	LX950	ocr-4(vs137) IV.	688 bp deletion (+ 1 bp insertion)
RAB7A	rab-7	VC308	rab-7(ok511)/mIn1 [mIs14 dpy-10(e128)] II.	741 bp deletion (+ 17 bp insertion); homozygous lethal
TFG	tfg-1	VC2125	tfg-1(ok2290)/hIn1 [unc-101(sy241)] I.	1264 bp deletion; homozygous lethal
HARS1	hars-1	tm4074	hars-1(tm4074) IV/nT1 [qIs51] (IV;V).	661 bp deletion; homozygous lethal
YARS1	yars-1	tm1490	yars-1(tm1490) I.	315 bp deletion; homozygous lethal
FGD4	exc-5	NJ731	exc-5(rh232) IV.	4564 bp deletion
PMP2	lbp-5	tm1618	lbp-5(tm1618) I.	940 bp deletion (+ 20 bp insertion)
MTMR2, SBF1, SBF2	mtm-1	WS3530	mtm-1(op309) I.	substitution (G > A; G106E)
	mtm-5	VC263	mtm-5(ok469) X.	665 bp deletion
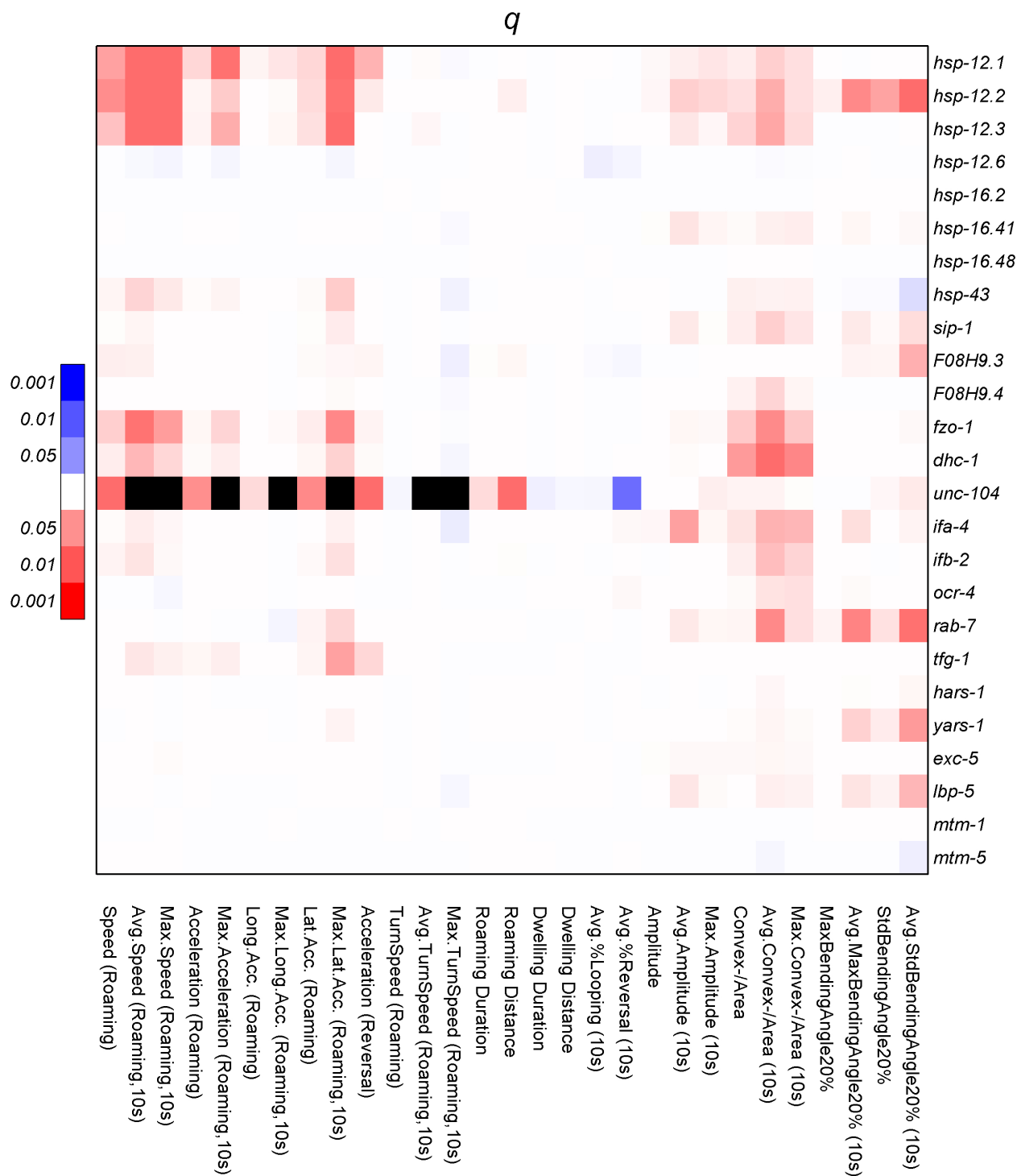
Fig. 2. A summary of locomotion and body posture phenotypes. Every square in this heat map indicates the *q*-value of the comparison of each behavioral feature (in columns) of each strain (in rows) to that of N2. It is color-coded in such a way that the color red indicates that N2 has a higher value than the mutant, while the color blue shows that N2 has a lower value than the mutant. The color becomes darker as the *q*-value decreases, which means that the difference is more significant. The color black indicates that the number of data was not sufficient to calculate a *q*-value (*unc-104* mutants had severe defects in locomotion, so they did not roam for 10 s). For the overlapping index η, see Supplementary Fig. S2. Avg., average; Std, standard deviation; Max., maximum; Lat., lateral; Acc., acceleration; Long., longitudinal.

of peripheral neuropathies (Table 1). For example, disruption of aminoacyl tRNA synthetases (*hars-1/HARS1, yars-1/YARS1*) was lethal to worms and homozygotes demonstrated larval arrest (Pierce et al., 2011; Sönnichsen et al., 2005), and therefore we had to test heterozygotes (*hars-1/+, yars-1/+*) instead.

Monitoring the behaviors of worms

We adapted WormTracker and its motion analysis workflow (Baek et al., 2002; Yemini et al., 2013). However, we largely simplified both the instrumentation and the analysis. The major difference is that our setup is much simpler without a software-controlled motorized XY-stage, because we do not track a single worm. Instead, our field of view covers an entire NGM plate (35 mm petri dish), and thus we can track 10 to 12 individuals simultaneously. This reduces the spatial resolution significantly (Fig. 1A), making a more sophisticated image analysis such as distinguishing head and tails, characterization of omega-turn, and upsilon-turn events impractical. However, even at the reduced resolution, we still can obtain movement trajectories (red curves in Fig. 1A) and body-skeleton curves (red curves in Fig. 1B) of individual worms.

From the trajectories and the body-skeleton curves, we quantified 44 motion features such as speed, acceleration, reversal, turn speed, roaming/dwelling intervals, and 60 body posture features such as amplitude, looping, and bending angles, as defined in the previous studies (Baek et al., 2002). Reversal is when worms make a rapid backward motion, as shown in Fig. 1A, and looping is when an animal's head or tail touches its body, making a loop. We will explain more of these features later in the text and in the supplementary text.

It should be noted that worms exhibit two-state moving behavior of roaming and dwelling (Ben Arous et al., 2009). As shown in Fig. 1A, worms sometimes spend their time in an inactive mode termed "dwelling" in which they do not move around much and only alternate backward and forward movement at a low speed, whereas they move fast in search of food in "roaming" mode. To disjoin the effect of the roaming/dwelling decision on worms' capacity to move, we need to compare the motion features in roaming and dwelling intervals separately.

Comparison of locomotion and shape features between strains

For each strain, we quantified each of the 104 behavioral features for all individuals in all images collected from the measurement. For each feature, we compared the distribution of each strain to that of N2, the *C. elegans* wild type, to determine if the two distributions are different from each other. Furthermore, we calculated the *q*-value for each comparison, following the same algorithm described in the literature (Storey, 2002; Yemini et al., 2013). Briefly, the *q*-value (positive false discovery rate) is a measure of how likely it is a false claim that the two distributions are different.

Fig. 2 summarizes the *q*-values of 29 selected behavioral features for all strains assayed in this study (See Supplementary Fig. S2 for the overlapping index η). We tried to include as many features as possible to illustrate a variety of different *q*-value patterns, while omitting those showing similar

patterns. The *q*-values of all 104 features are provided in Supplementary Material. In Fig. 2, it is notable that *hsp-12.1, hsp-12.2*, and *hsp-12.3/HSPB1* mutants exhibit deficiency in their motion: they move slower in roaming intervals (speed, average speed over 10 s, maximum speed over 10 s) and they also accelerate slower (maximum lateral acceleration over 10 s). Since worms tend to keep their speed while they are roaming, the difference in the acceleration capacity is better observed in lateral acceleration as they change directions. Other strains that move slower than N2 are *fzo-1/MFN2, dhc-1/DYNC1H1*, and *unc-104/KIF1B* mutants. In Fig. 3, the boxplots of these strains illustrate their differences with N2 in detail (Figs. 3A and 3B). *unc-104* worms looked physically abnormal under our experiment conditions: they did not roam and their locomotion was very limited. *hsp-43/HSPB1* and *tfg-1/TFG* mutants were other strains that showed decreased lateral acceleration (maximum lateral acceleration over 10 s).

Body posture features of *hsp-12.1, hsp-12.2*, and *hsp-12.3/HSPB1* deficient mutants were also significantly different from those of N2. The amplitude of the lateral undulling motion that worms make while they crawl (Fig. 3E) and the related body posture features such as the ratio of the area of convex hull of worm image (Convex-Area) to the area of worm image (Convex-Area/Area) are smaller for these worms than those of N2 (Fig. 3C). This means that these worms appear to be relatively straight. Other than the *HSPB1* homologues, *fzo-1/MFN2, dhc-1/DYNC1H1, ifa-4, ifb-2/NEFL*, and *rab-7/RAB7A* also have smaller amplitude than N2.

The body of *hsp-12.2/HSPB1* deficient mutant is less bent than that of N2. To quantify this, we calculated a bending angle, the angle between two tangential vectors separated by 20% of body length, for every pair over the body (Fig. 3F). Its maximum ('maximum bending angle 20%') indicates how much the body is bent where it is bent the most, while its standard deviation ('standard deviation of bending angle 20%') measures how much the bending angle changes at different parts of the body. Not only the maximum bending angle but also the standard deviation of the bending angles are smaller in the *hsp-12.2/HSPB1* mutant (Fig. 3D). The body of *rab-7/RAB7A* and *yars-1/YARS1* deficient worms are also less bent than N2.

Figs. 3A-3D present boxplots of several selected strains that exhibit differences both in locomotion and body posture features. The boxplots of corresponding behavioral features for all strains are available in Supplementary Figs. S3-S6, respectively.

DISCUSSION

Animal models are powerful tools for studying the pathogenic mechanisms of peripheral neuropathies as well as for finding therapeutic strategies (d'Ydewalle et al., 2011; Hong et al., 2016; Won et al., 2019; Yamaguchi and Takashima, 2018). Nevertheless, *C. elegans* models have rarely been applied until recently.

In an effort to find novel *C. elegans* peripheral neuropathy models, we monitored behaviors of various worms with mutation of *C. elegans* homologues of the causative genes and compiled a database of their behavioral features, adapting
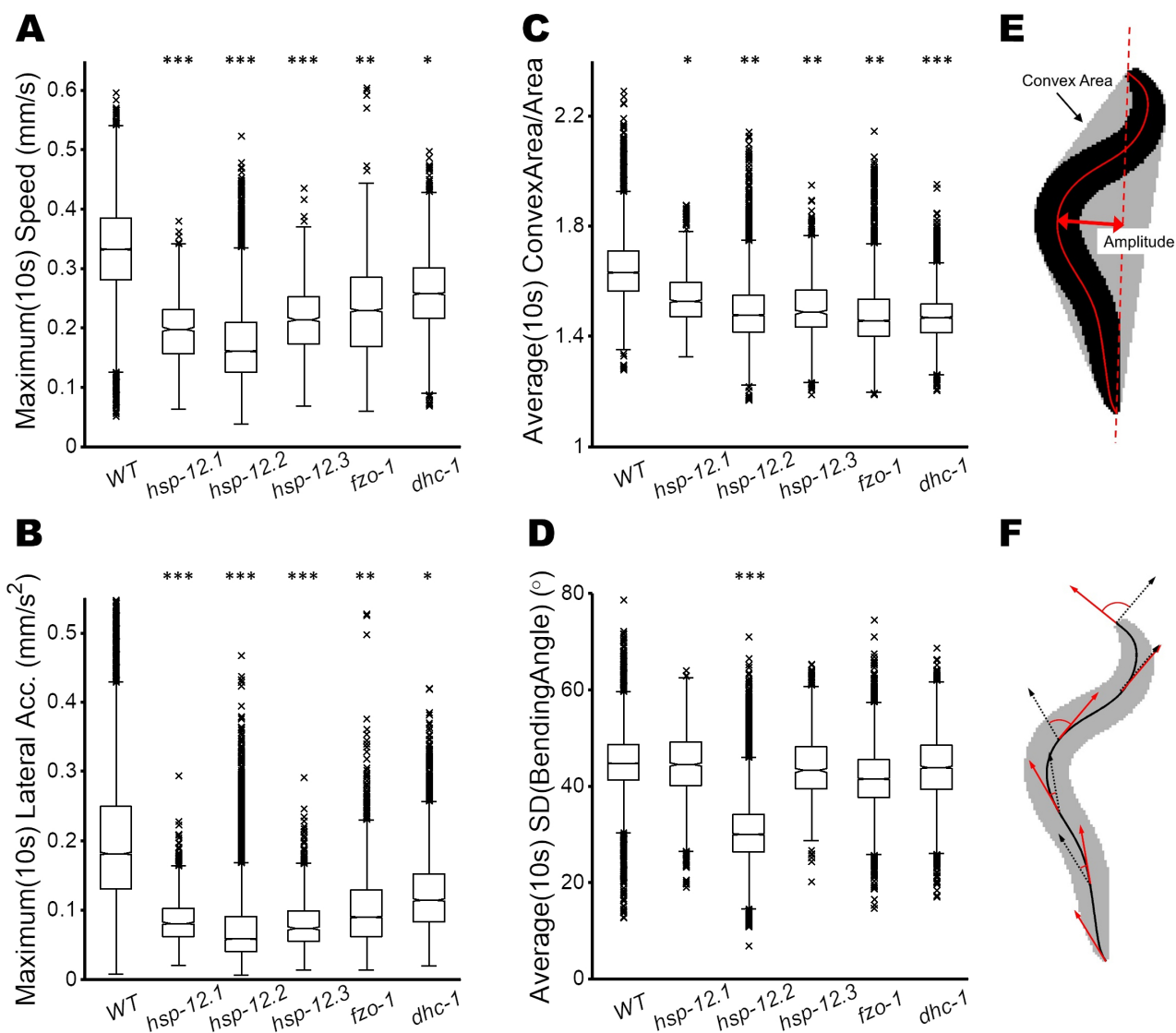
Fig. 3. Boxplots of selected behavioral features. Boxplots of *hsp-12.1*, *hsp-12.2*, *hsp-12.3*, *fzo-1*, and *dhc-1* mutants and of the wild type for (A) maximum speed in 10 s, (B) maximum lateral acceleration in 10 s, (C) convex area/area (the ratio of the area of convex hull of the worm to the area), averaged over 10 s, and (D) standard deviation of bending angles over the body, averaged over 10 s. On each box, the bottom, the center, and the top edges indicate 25th, 50th, and 75th percentiles, respectively. Significant differences compared to the wild type are shown in asterisks ($*P < 0.05$, $**P < 0.01$, and $***P < 0.001$). (E) Convex-area and amplitude: the worm's convex-area is the area of the gray (and the black) region. The amplitude is the farthest distance from the line that connects the head and the tail. (F) Bending angles: the angle between two tangential vectors (red and black) at two positions separated by 20% of the body length. Bending angles are defined at every such position pair.

previous studies on an automated system for monitoring worms' behavior (Baek et al., 2002; Yemini et al., 2013).

Among 11 different *C. elegans* homologues of *HSPB1* that already had their deletion mutants ready in the CGC and NBRP, *hsp-12.1*, *hsp-12.2*, and *hsp-12.3* deficient worms exhibit a significant decrease in their locomotion capacity, making these worms viable candidates for a *C. elegans* peripheral neuropathy model.

These worms also exhibit a different body posture compared to the *C. elegans* wild type. The body posture of worms

is indeed a neurogenetic phenotype in worms: for example, the amplitude of lateral undulation of worms is regulated by a mechano-sensory neuron DVA (Zhen and Samuel, 2015). The amplitude has been linked to the speed of locomotion in a previous biophysical study (Shen et al., 2012). Bending angles across the body are also coordinated by excitatory ventral cord motor neurons (Wen et al., 2018).

Other reasonable candidates would be *fzo-1/MFN2*, *dhc-1/DYNC1H1*, and *unc-104/KIF1B*. In fact, *fzo-1* mutant has already been employed to examine the role of mitochondrial

dynamics on behavior and lifespan (Byrne et al., 2019). Also, it was reported that axonal transport in *unc-104* worms was impaired and the worms were much slower and underwent larval arrest depending on the growth temperature (Edwards et al., 2015). Dynein (*DYNC1H1*) as well as kinesin (*KIF1A, KIF1B*) is also involved in axonal transport.

Ubiquitously expressed small heat shock protein 27 (HSP27), which is encoded by *HSPB1*, protects cells from a wide variety of unfavorable physiological and environmental conditions (Acunzo et al., 2012). Mutations in human *HSPB1* are associated with CMT2F and dHMN2B (Evgrafov et al., 2004), and mouse HspB1 mutants showed distal axonal loss and a decrease in acetylated alpha-tubulin in peripheral nerves (d'Ydewalle et al., 2011). Mutations in *MFN2*, which develop dominant or recessive CMT2A, are known as the most common genetic causes of axonal CMT (Züchner et al., 2004). MFN2 mediates the dynamic balance between fusion and fission of mitochondria (Santel and Fuller, 2001). *DYNC1H1*, implicated to CMT2O (Weedon et al., 2011), encodes a large subunit of the cytoplasmic dynein complex, which is a type of microtubule-activated ATPase. Mutations in this gene caused neurodegeneration, anterior horn cell death, impairment of axonal retrograde transport, and perturbation of neuronal development and migration (Hafezparast et al., 2003). *KIF1B*, related to CMT2A1 (Zhao et al., 2001), encodes an N-terminal-type motor protein that plays an important role in the anterograde transport of mitochondria as a monomeric motor. Mouse Kif1b heterozygotes showed defects in transporting synaptic vesicle precursors and progressive muscle weakness (Zhao et al., 2001).

To conclude, we suggest *C. elegans* homologues of *HSPB1*, *MFN2*, *DYNC1H1*, and *KIF1B* as a model for axonal peripheral neuropathies. We hope that our behavioral phenotype database will assist the development of more *C. elegans* models for better understanding of pathogenesis mechanisms as well as novel therapeutic strategies.

Note: Supplementary information is available on the Molecules and Cells website (www.molcells.org).

AUTHOR CONTRIBUTIONS
K.W.C. and K.S.L. wrote the manuscript. K.S.L. designed the experiment and K.S.L. and J.S.K. performed the experiment. K.S.L. performed the image analysis and statistical analysis.

CONFLICT OF INTEREST
The authors have no potential conflicts of interest to disclose.

ORCID
Ki Wha Chung	https://orcid.org/0000-0003-0363-8432
Ju Seong Kim	https://orcid.org/0000-0002-6298-977X
Kyung Suk Lee	https://orcid.org/0000-0003-4157-5153

REFERENCES

Acunzo, J., Katsogiannou, M., and Rocchi, P. (2012). Small heat shock proteins HSP27 (HspB1), αB-crystallin (HspB5) and HSP22 (HspB8) as regulators of cell death. Int. J. Biochem. Cell Biol. *44*, 1622-1631.

Antonellis, A., Ellsworth, R.E., Sambuughin, N., Puls, I., Abel, A., Lee-Lin, S.Q., Jordanova, A., Kremensky, I., Christodoulou, K., Middleton, L.T., et al. (2003). Glycyl tRNA synthetase mutations in Charcot-Marie-Tooth disease type 2D and distal spinal muscular atrophy type V. Am. J. Hum. Genet. *72*, 1293-1299.

Baek, J.H., Cosman, P., Feng, Z., Silver, J., and Schafer, W.R. (2002). Using machine vision to analyze and classify *Caenorhabditis elegans* behavioral phenotypes quantitatively. J. Neurosci. Methods *118*, 9-21.

Ben Arous, J., Laffont, S., and Chatenay, D. (2009). Molecular and sensory basis of a food related two-state behavior in *C. elegans*. PLoS One *4*, e7584.

Bragato, C., Gaudenzi, G., Blasevich, F., Pavesi, G., Maggi, L., Giunta, M., Cotelli, F., and Mora, M. (2016). Zebrafish as a model to investigate dynamin 2-related diseases. Sci. Rep. *6*, 20466.

Brenner, S. (1974). The genetics of *Caenorhabditis elegans*. Genetics *77*, 71-94.

Byrne, J.J., Soh, M.S., Chandhok, G., Vijayaraghavan, T., Teoh, J.S., Crawford, S., Cobham, A.E., Yapa, N.M.B., Mirth, C.K., and Neumann, B. (2019). Disruption of mitochondrial dynamics affects behaviour and lifespan in *Caenorhabditis elegans*. Cell. Mol. Life Sci. *76*, 1967-1985.

d'Ydewalle, C., Krishnan, J., Chiheb, D.M., Van Damme, P., Irobi, J., Kozikowski, A.P., Vanden Berghe, P., Timmerman, V., Robberecht, W., and Van Den Bosch, L. (2011). HDAC6 inhibitors reverse axonal loss in a mouse model of mutant HSPB1-induced Charcot-Marie-Tooth disease. Nat. Med. *17*, 968-974.

Edwards, S.L., Yorks, R.M., Morrison, L.M., Hoover, C.M., and Miller, K.G. (2015). Synapse-assembly proteins maintain synaptic vesicle cluster stability and regulate synaptic vesicle transport in *Caenorhabditis elegans*. Genetics *201*, 91-116.

England, J.D. and Asbury, A.K. (2004). Peripheral neuropathy. Lancet *363*, 2151-2161.

Eschenbacher, W.H., Song, M., Chen, Y., Bhandari, P., Zhao, P., Jowdy, C.C., Engelhard, J.T., and Dorn, G.W., 2nd (2012). Two rare human mitofusin 2 mutations alter mitochondrial dynamics and induce retinal and cardiac pathology in Drosophila. PLoS One *7*, e44296.

Evgrafov, O.V., Mersiyanova, I., Irobi, J., Van Den Bosch, L., Dierick, I., Leung, C.L., Schagina, O., Verpoorten, N., Van Impe, K., Fedotov, V., et al. (2004). Mutant small heat-shock protein 27 causes axonal Charcot-Marie-Tooth disease and distal hereditary motor neuropathy. Nat. Genet. *36*, 602-606.

Hafezparast, M., Klocke, R., Ruhrberg, C., Marquardt, A., Ahmad-Annuar, A., Bowen, S., Lalli, G., Witherden, A.S., Hummerich, H., Nicholson, S., et al. (2003). Mutations in dynein link motor neuron degeneration to defects in retrograde transport. Science *300*, 808.

Harris, T.W., Arnaboldi, V., Cain, S., Chan, J., Chen, W.J., Cho, J., Davis, P., Gao, S., Grove, C.A., Kishore, R., et al. (2020). WormBase: a modern model organism information resource. Nucleic Acids Res. *48*, D762-D767.

Hong, Y.B., Kang, J., Kim, J.H., Lee, J., Kwak, G., Hyun, Y.S., Nam, S.H., Hong, H.D., Choi, Y.R., Jung, S.C., et al. (2016). DGAT2 mutation in a family with autosomal-dominant early-onset axonal Charcot-Marie-Tooth disease. Hum. Mutat. *37*, 473-480.

Inman, H.F. and Bradley, E.L., Jr. (1989). The overlapping coefficient as

a measure of agreement between probability distributions and point estimation of the overlap of two normal densities. Commun. Stat. Theory Methods *18*, 3851-3874.

Jordanova, A., Irobi, J., Thomas, F.P., Van Dijck, P., Meerschaert, K., Dewil, M., Dierick, I., Jacobs, A., De Vriendt, E., Guergueltcheva, V., et al. (2006). Disrupted function and axonal distribution of mutant tyrosyl-tRNA synthetase in dominant intermediate Charcot-Marie-Tooth neuropathy. Nat. Genet. *38*, 197-202.

Kim, J.Y., Woo, S.Y., Hong, Y.B., Choi, H., Kim, J., Choi, H., Mook-Jung, I., Ha, N., Kyung, J., Koo, S.K., et al. (2016). HDAC6 Inhibitors rescued the defective axonal mitochondrial movement in motor neurons derived from the induced pluripotent stem cells of peripheral neuropathy patients with HSPB1 mutation. Stem Cells Int. *2016*, 9475981.

Lee, A.J., Nam, D.E., Choi, Y.J., Nam, S.H., Choi, B.O., and Chung, K.W. (2020). Alanyl-tRNA synthetase 1 (AARS1) gene mutation in a family with intermediate Charcot-Marie-Tooth neuropathy. Genes Genomics *42*, 663-672.

Lee, H.J., Park, J., Nakhro, K., Park, J.M., Hur, Y.M., Choi, B.O., and Chung, K.W. (2012). Two novel mutations of GARS in Korean families with distal hereditary motor neuropathy type V. J. Peripher. Nerv. Syst. *17*, 418-421.

Long, R.T., Peng, J.B., Huang, L.L., Jiang, G.P., Liao, Y.J., Sun, H., Hu, Y.D., and Liao, X.H. (2019). Augmenter of liver regeneration alleviates renal hypoxia-reoxygenation injury by regulating mitochondrial dynamics in renal tubular epithelial cells. Mol. Cells *42*, 893-905.

Mattingly, B.C. and Buechner, M. (2011). The FGD homologue EXC-5 regulates apical trafficking in *C. elegans* tubules. Dev. Biol. *359*, 59-72.

Nam, S.H., Hong, Y.B., Hyun, Y.S., Nam, D.E., Kwak, G., Hwang, S.H., Choi, B.O., and Chung, K.W. (2016). Identification of genetic causes of inherited peripheral neuropathies by targeted gene panel sequencing. Mol. Cells *39*, 382-388.

Pareyson, D., Saveri, P., and Pisciotta, C. (2017). New developments in Charcot-Marie-Tooth neuropathy and related diseases. Curr. Opin. Neurol. *30*, 471-480.

Pastore, M. and Calcagnì, A. (2019). Measuring distribution similarities between samples: a distribution-free overlapping index. Front. Psychol. *10*, 1089.

Pierce, S.B., Chisholm, K.M., Lynch, E.D., Lee, M.K., Walsh, T., Opitz, J.M., Li, W., Klevit, R.E., and King, M.C. (2011). Mutations in mitochondrial histidyl tRNA synthetase HARS2 cause ovarian dysgenesis and sensorineural hearing loss of Perrault syndrome. Proc. Natl. Acad. Sci. U. S. A. *108*, 6543-6548.

Santel, A. and Fuller, M.T. (2001). Control of mitochondrial morphology by a human mitofusin. J. Cell Sci. *114*, 867-874.

Schwartz, N.U. (2019). Charcot-Marie-Tooth 2F (Hsp27 mutations): a review. Neurobiol. Dis. *130*, 104505.

Shen, X.N., Sznitman, J., Krajacic, P., Lamitina, T., and Arratia, P.E. (2012). Undulatory locomotion of *Caenorhabditis elegans* on wet surfaces. Biophys. J. *102*, 2772-2781.

Sönnichsen, B., Koski, L.B., Walsh, A., Marschall, P., Neumann, B., Brehm, M., Alleaume, A.M., Artelt, J., Bettencourt, P., Cassin, E., et al. (2005). Full-genome RNAi profiling of early embryogenesis in *Caenorhabditis elegans*. Nature *434*, 462-469.

Storey, J.D. (2002). A direct approach to false discovery rates. J. R. Stat. Soc. Series B Stat. Methodol. *64*, 479-498.

Tanaka, Y. and Hirokawa, N. (2002). Mouse models of Charcot-Marie-Tooth disease. Trends Genet. *18*, S39-S44.

Vester, A., Velez-Ruiz, G., McLaughlin, H.M., NISC Comparative Sequencing Program, Lupski, J.R., Talbot, K., Vance, J.M., Züchner, S., Roda, R.H., Fischbeck, K.H., et al. (2013). A loss-of-function variant in the human histidyl-tRNA synthetase (HARS) gene is neurotoxic in vivo. Hum. Mutat. *34*, 191-199.

Weedon, M.N., Hastings, R., Caswell, R., Xie, W., Paszkiewicz, K., Antoniadi, T., Williams, M., King, C., Greenhalgh, L., Newbury-Ecob, R., et al. (2011). Exome sequencing identifies a DYNC1H1 mutation in a large pedigree with dominant axonal Charcot-Marie-Tooth disease. Am. J. Hum. Genet. *89*, 308-312.

Wen, Q., Gao, S., and Zhen, M. (2018). *Caenorhabditis elegans* excitatory ventral cord motor neurons derive rhythm for body undulation. Philos. Trans. R. Soc. Lond. B Biol. Sci. *373*, 20170370.

Won, S.Y., Choi, B.O., Chung, K.W., and Lee, J.E. (2019). Zebrafish is a central model to dissect the peripheral neuropathy. Genes Genomics *41*, 993-1000.

Wright, M.W., Eyre, T.A., Lush, M.J., Povey, S., and Bruford, E.A. (2005). HCOP: the HGNC comparison of orthology predictions search tool. Mamm. Genome *16*, 827-828.

Yamaguchi, M. and Takashima, H. (2018). Drosophila Charcot-Marie-Tooth disease models. Adv. Exp. Med. Biol. *1076*, 97-117.

Yemini, E., Jucikas, T., Grundy, L.J., Brown, A.E., and Schafer, W.R. (2013). A database of *Caenorhabditis elegans* behavioral phenotypes. Nat. Methods *10*, 877-879.

Zhao, C., Takita, J., Tanaka, Y., Setou, M., Nakagawa, T., Takeda, S., Yang, H.W., Terada, S., Nakata, T., Takei, Y., et al. (2001). Charcot-Marie-Tooth disease type 2A caused by mutation in a microtubule motor KIF1Bbeta. Cell *105*, 587-597.

Zhen, M. and Samuel, A.D. (2015). *C. elegans* locomotion: small circuits, complex functions. Curr. Opin. Neurobiol. *33*, 117-126.

Züchner, S., Mersiyanova, I.V., Muglia, M., Bissar-Tadmouri, N., Rochelle, J., Dadali, E.L., Zappia, M., Nelis, E., Patitucci, A., Senderek, J., et al. (2004). Mutations in the mitochondrial GTPase mitofusin 2 cause Charcot-Marie-Tooth neuropathy type 2A. Nat. Genet. *36*, 449-451.